Construction and Building Materials 298 (2021) 123758

Contents lists available at ScienceDirect

Construction and Building Materials

journal homepage: www.elsevier.com/locate/conbuildmat

Implementation of capillary penetration coefficient on water sorptivity for porous building materials: An experimental study

A. El Abd [a], M. Taman [b,*], S.E. Kichanov [c], E. Hamad [a], K.M. Nazarov [c,d]

[a] Reactor Physics Department, Nuclear Research Center, Egyptian Atomic Energy Authority, 13759 Abu Zaabal, Egypt
[b] Department of Structural Engineering, Faculty of Engineering, Tanta University, 31511 Tanta, Egypt
[c] Frank Laboratory of Neutron Physics, Joint Institute for Nuclear Research, 141980 Dubna, Russia
[d] Eurasian National University, 010008 Astana, Kazakhstan

HIGHLIGHTS

- Sorptivity is directly proportional to capillary penetration coefficient for brick samples.
- Capillary water absorption coefficients for building materials can be predicted.
- Acrylic paints decrease the capillary absorption processes more than the sultry adhesive coat.
- Capillary absorption processes depend on the sealing materials.

ARTICLE INFO

Article history:
Received 6 February 2021
Received in revised form 22 May 2021
Accepted 24 May 2021

Keywords:
Neutron radiography
Bricks
Capillary coefficient
Sorptivity
Porosity
Water front
Profiles

ABSTRACT

Neutron radiography is used to study the relation between water sorptivities (s) and capillary penetration coefficient (k), and to reveal impacts of sealing method on the water absorption process in brick samples. Except for the ends, the samples' outer surfaces were coated with a polymeric waterproofing slurry. While the samples were absorbing water, neutron radiography images were recorded continuously. Analyses of the acquired images, as well as published results for construction building materials, were used to determine water sorptivities (s), capillary penetration coefficient (k), and capillary porosity (θ_c). The results showed that s is proportional to k in a direct manner, and that θ_c is the proportionality constant. It was found that samples coated with a polymeric waterproofing slurry absorb water more quickly than samples coated with acrylic paint.

1. Introduction

Chemical and biological agents transported by water are regarded as major factors in the degradation of building materials. Capillarity transports water in building materials like bricks [1–3]. The Lucas–Washburn equation [4] is commonly used to describe capillary water absorption:

$$h = kt^{1/2} + a \quad (1)$$

where h is height of the liquid front (cm), t is the absorption time (h), the intercept a is a correction term which accounts for surface effects and k is the capillary penetration coefficient (cm.h$^{-1/2}$). Sorptivity s (cm. h$^{-1/2}$) is determined according to

$$I = W/A = St^{1/2} + b \quad (2)$$

where I is the cumulative water absorption (cm), W is the volume of water absorbed (cm^3), A is the sample surface area exposed to water (cm^2), and the intercept b is a correction term [5] to account for surface effects [5]. k and S are parameters characterizing capillary flow process in porous media and are functions of both the liquid properties (surface tension, contact angle, the dynamic viscosity) and the porous medium matrix (the pore structure). Both equations (1) and (2) are used to describe water absorption in construction building materials. The intercepts a and b may take positive or negative values. Positive intercepts indicate rapid filling of the pores near the surface of sample immersed in water during the initial period of water absorption. Negative intercepts indicate a delay or acceleration of capillary absorption ([5] and references cited in). The sorpitivity can be determined easily by gravimetric method while the capillary penetration coefficient

* Corresponding author.
E-mail address: mohamed.taman@f-eng.tanta.edu.eg (M. Taman).

https://doi.org/10.1016/j.conbuildmat.2021.123758
0950-0618/

can be determined by visualization of the movement of water inside a porous sample using neutron and/or x-ray radiography methods [6,7].

Neutron radiography (NR) is based on recording a neutron beam after absorption and scattering (attenuation) by an object investigated by a suitable detector (CCD camera) [8]. Since thermal neutrons are strongly scattered by water due to the large scattering cross-section for Hydrogen atoms, NR is considered a powerful tool to study water absorption in porous media. NR has been used to study water absorption processes in a variety of building materials (see for example [9–15]).

There is some data on the relation between k and S. Hanžič, and Ilić, 2003 [16] determined capillary coefficients for water and fuel oil in three different types of concrete using neutron radiography. The determined capillary coefficient values were compared with the sorptivity measured by the gravimetric method. They showed that the ratio between k and s for water are 5.5 ± 0.6, 5.8 ± 0.6 and 7.1 ± 0.7 in concrete without additives, concrete with an air entraining agent and concrete with a plasticizer, respectively. Yang et al., 2019 [17] used X-ray CT combined with CsCl enhancing to investigate the relationship between k and s of water for mortar and concrete samples. The results showed that the ratio (s/k) equals the values of porosity (θ_c) determined by vacuum water-saturated method of the samples investigated. Zhang et al., 2011 [18] used neutron radiography to study the process of water absorption in two types of concretes with different water–cement ratios (0.4 and 0.6). The results for s, k and θ_c were correlated as $s = \rho\theta_c k$ (where ρ is the liquid density). The reported values for θ_c were 0.059 and 0.087 for concrete with w/c ratio 0.4 and 0.6, respectively. Those values are higher than the corresponding ones extracted from the water profiles (~0.034 and ~ 0.047).

These results were not confirmed by other studies in literature. Additionally, there are no studies in literature for the relationship between s and k for brick samples. Thus, data are required to investigate the relationship between s and k for brick samples. Therefore, further analyses of reported results for other building materials such as mortars, pastes, bricks and some rocks are needed.

To reduce evaporation and allow liquid to flow in one direction during capillary absorption tests, the lateral sides of the sample are often sealed with a sealing material. The effect of the sealing method on capillary water absorption tests has not been extensively studied. It has been reported that the capillary absorption process may depend on the sealing method for some types of porous samples. Moreover, it could perturb the process of capillary water absorption ([5] and references cited in). Such hypotheses were not confirmed by other studies. Thus, the impact of the sealing method on capillary water absorption processes needs further studies.

The aim of the present work is to use neutron radiography to: 1) determine the relationship between the capillarity penetration coefficient and sorptivity for brick samples. The sorptivity is determined by neutron radiography, and 2) investigate the impact of the sealing method on capillary water absorption process. In this work, the NR station installed at the 14th beam line of the IBR-2 reactor, Joint Institute of Nuclear Research, JINR, (Dubna), Russia was used to perform the experiments.

2. Experimental details and measurements

The NR station installed at the 14th beam line of the pulsed reactor IBR-2, Joint Institute for Nuclear Research (JINR), Dubna, Russia [19,20] was used to perform the experiments. The L/D ratio for the collimator is 200. The length L = 1000 cm, the pinhole diameter D = 5 cm. It is classical standard linear pinhole-type collimator. It consists of four cylindrical divergent inserts of boron-contained polyethylene disks and steel rings for construction rigidity. The collimator holes expand in diameter from initial 5.0 to 23.7 cm (it is not radial or reflector collimator). The source (reactor moderator wall) to sample distance is 2200 cm, the sample-to-scintillator length is 1 cm. The thermal neutron flux at the position of the sample is $5.5\text{x}10^6$ n.cm^{-2}.s^{-1} and the detector system is based on a ^{6}LiF/ZnS scintillation screen. A CCD camera was used to record images and the average spatial image resolution is ~ 300 μm. Dark current images were subtracted from the registered NR images, then those were normalized with respect to an image for the incident white neutron beam. Further analysis was carried out using the Image J software [21].

Water absorption into three kinds of brick samples was investigated by NR. The samples are cement light weight (brick 1), clay (brick 2) and sand-lime light weight (brick 3). More details about these samples were reported in El Abd el al., 2020 [12]. These samples besides another sample (brick 4) were previously investigated by NR [12]. However, an acrylic paint was used as a sealing agent [12]. The dimensions of the brick samples (thickness × width × length) investigated in this work are: 2 cm x3.3 cm × 9 cm, 1.65 cm x3 cm x9.5 cm, and 2.4 cm x2.4 cm x10 cm, respectively. The samples were oven dried for several days at 105 ^{0}C. These samples are shorter in length than those previously investigated [12]. In this work, the surfaces of the samples investigated, along the water flow direction (four sides), were coated with a polymeric waterproofing slurry except their ends that characterized with small cross section areas. This waterproofing slurry was used as a sealing agent to allow water to flow in one direction (along the length of the samples) and prevent water evaporation during the water absorption experiments. Two perpendicular layers of the slurry coat, with total thicknesses less than 2 mm, were applied after the specimens were wetted using clean water by stiff brush. The samples are dried again for several days. The NR experiment was carried out during the capillary water absorption test for the samples prepared. The samples were fixed vertically and their ends were immersed in a water container. The samples absorb water from the bottom ends by capillary forces. The level of water in the container covers ~ 3 mm of the immersed sample ends and was kept constant. Several NR images were registered continuously during the water absorption process.

Corrections for the neutron scattering arising from both the samples and water absorbed during water absorption process were carried out using the procedures previously used in El Abd et al., 2020 [12]. In this work, these procedures used cadmium (Cd) strips. Cd absorbs incident thermal neutrons on it, since it has a large absorption cross section for thermal neutrons. Thus, if a Cd strip was stacked on the surface of a sample along its length, such that Cd is exposed to a thermal neutron beam, the value of neutron intensity under Cd would just be due to the scattered neutrons. The neutron intensity, I_b after passing a dry brick sample is given by

$$I_b = I_o \exp(-\sum_b L_b) + I_{sb} \quad (3)$$

where I_0 is the neutron intensity without the sample, L_b is the sample thickness (cm), $\sum_b$ (cm^{-1}) is the effective macroscopic cross section for the brick sample, andI_{sb} is a neutron scattering component resulting from the brick sample. The transmitted neutrons from a wetted sample, I_{b+w} is given by

$$I_{b+w} = I_o \exp(-\sum_b L_b - \sum_w L_w) + I_{sb} + I_{sw} \quad (4)$$

where L_w is the water thickness (cm), $\sum_w$ (cm^{-1}) is the effective macroscopic cross section for water, I_{sw} is the neutron scattering component resulting from water inside the brick sample. Under

Cd, the neutron intensities for the dry and wetted sample are given by

$$(I_b)_{cd} = I_{sb} \quad 5$$

and

$$(I_{b+w})_{cd} = I_{sb} + I_{sw} \quad 6$$

respectively. From Equations 3–6, the water thickness L_w at a given position along the water flow direction, x and at an absorption time, t is given by

$$L_w(x,t) = \frac{1}{\sum_w} \ln\left(\frac{I_b - I_{sb}}{I_{b+w} - (I_{sb} + I_{sw})}\right) \quad 7$$

The volumetric water content at any position × and time t along the water flow direction is given by

$$\theta(x,t) = \frac{L_w(x,t)}{L_b} \quad 8$$

The total volume of water absorbed along the flow direction to a distance × (cm) is given by

$$\int_0^x L_w(x,t)\ \ L_t\ dx = \int_0^x \frac{L_t}{\sum_w} \ln\left(\frac{I_b - I_{sb}}{I_{b+w} - (I_{sb} + I_{sw})}\right) dx \quad 9$$

where L_t(cm) is the width of the sample. The total volume I, of water absorbed divided by the sample surface area L_bxL_t (cm^2) exposed to water in unites of cm is given by

$$I = \int_0^x \theta(x,t)\ dx = \int_0^x \frac{1}{L_b \sum_w} \ln\left(\frac{I_b - I_{sb}}{I_{b+w} - (I_{sb} + I_{sw})}\right) dx \quad 10$$

where $\theta(x,t) = \frac{L_w(x,t)}{L_b}$, is the volumetric water content at any position x and time t along the water flow direction. The integral $\int_0^x \theta(x,t)\ dx$ is the cumulative water absorption, I given by Eq. (2). In terms of the square root of the absorption time $\sqrt{t}$, equation (10) can be used to determine the sorpitivity. I (I = $\int_0^x \theta(x,t)\ dx$) is determined from the water profiles at the different absorption times t, then I is plotted versus $\sqrt{t}$. The I- $\sqrt{t}$ results should be fitted with straight line equation, the slope of which is the sorptivity S. This means that I should follow $\sqrt{t}$ behavior.

3. Results and discussion

3.1. Determination of capillary penetration coeffiecients

Some of the NR images registered for brick samples 1, 2 and 3 during the capillary water absorption process are shown in Fig. 1a. It is possible to notice that water advances clearly in the samples investigated as the absorption time elapses. The wetted regions in the images are darker than the dry ones. Sharp water fronts can be noticed between the wetted and dry regions of the samples investigated. The very dark regions along the length of the samples (direction of water flow) are due to the Cd strips attached to the samples. It can be observed for brick 1 and 2 samples that the advances of water (penetrated distances) are comparable. Very slow water absorption into brick 3 can be noticed in comparison with the other samples.

Two rectangular areas were drawn through the NR images acquired along the direction of water flow for the investigated samples. One was drawn on the shadow of the Cd strip and the other one beside it. For clarity, these rectangles are shown in the first image shown in Fig.1a at an absorption time 3.43 min for the brick 1 sample. These rectangles were used to extract the neutron intensity components I_b, I_{sb} ,$I_{b+w}$and I_{sw}. Such components were used for determining the water content distribution inside the samples as the absorption time elapses (water profiles) using Equation (8).

The extracted water profiles for bricks 1, brick 2 and brick 3 samples are shown in Figs. 2a, 3a and 4a, respectively. From these profiles, the water front positions as the absorption time elapses were determined at two values for the water contents (atθ = 0 and 0.125). The results are shown in Figs. 2b, 3b and 4b, respectively. The results were fitted with straight line equations. As one can see, the water fronts follow the $\sqrt{t}$ behavior with positive intercepts (equation (1)). Table 1 lists the values of the slopes, k (the capillary coefficients) corresponding toθ = 0 and 0.125 for brick samples 1, 2 and 3. For comparison of the results, Table 1 lists the values of k for the same brick samples (1, 2, 3, and 4) which were measured previously[12]- the brick 4 sample was not measured in the current work.

We reanalyzed the NR images of for brick 3 sample which was previously presented in El Abd et al., [12] since the progress of the water front inside it was irregular during the water absorption test. Fig. 1b shows some NR images for brick 3 as the absorption time elapses. Two rectangular areas were drawn as shown in Fig. 1b (at the absorption time T = 45.25 min) to determine the water profiles and then determining the water front positions as the absorption time elapses. One rectangle was drawn beside the Cd strip (region 1) and the second was drawn near the edge of the sample (region 2). The results are shown in Fig. 5 forθ = 0, 0.1 ,0.15 and 0.2. Although values of the water front positions near edge (region 2) of the sample are higher than those near the Cd-strip (region 1), water proceeds in region 1 faster than in region 2. This is probably due to the acrylic paint used to seal the samples. The capillary coefficients values are listed in Table 1. While the values of k in region 1 increase as θ increases, they are approximately comparable for region 2.

The capillary coefficients determined in the present work were compared with those values in El Abd et al., 2020 [12] (Table1). They are higher by factors of 1.47 and 1.58 for brick 1 and brick 2, respectively. For brick 3 samples, the ratios of the average values of k in the present work with respect to those for regions 1 and 2 (reg-1and reg- 2)– Table 1 – are 1.16 and 1.59, respectively. The higher values of k compared to those in the previous study can be attributed to the sealing material used. The acrylic paint penetrates deeper into the samples than the polymeric waterproofing slurry, likely reducing the effective cross-section size for the capillary absorption process. Thus, capillary water absorption processes depend on the sealing material. There are very limited results in literature for the effect of the sealing method on the capillary water absorption [5].

3.2. Determination of sorptivty and capillary porosity

The sorptivity was determined for the samples investigated using Eq. (10). The cumulative water absorbed (I) was determined using the results of θ versus x at the different absorption times for each of the samples investigated. The plots of I versus $\sqrt{t}$ are shown in Fig. 6 for brick 1, 2, and 3 samples. Fig. 6 also shows the results for the same samples, which were previously investigated [12]. It is noticeable that the values of I follow $\sqrt{t}$ behavior. The slopes of the straight-line fits are the sorptivities – Table 1. The values of sorptivities determined in the present work are higher than the corresponding ones in the previous work [12]. This confirms the dependence of the capillary water absorption process on the sealing material.

The capillary porosity θ_c is defined in this work as the water content near surface of the water container (x ~ 0). Values of θ_c were determined from the water profiles for the samples investigated (Table 1). The ratios, $k_c = s/\theta_c$ were calculated. The calculated values of k_c (predicted) are in agreement with the experi-

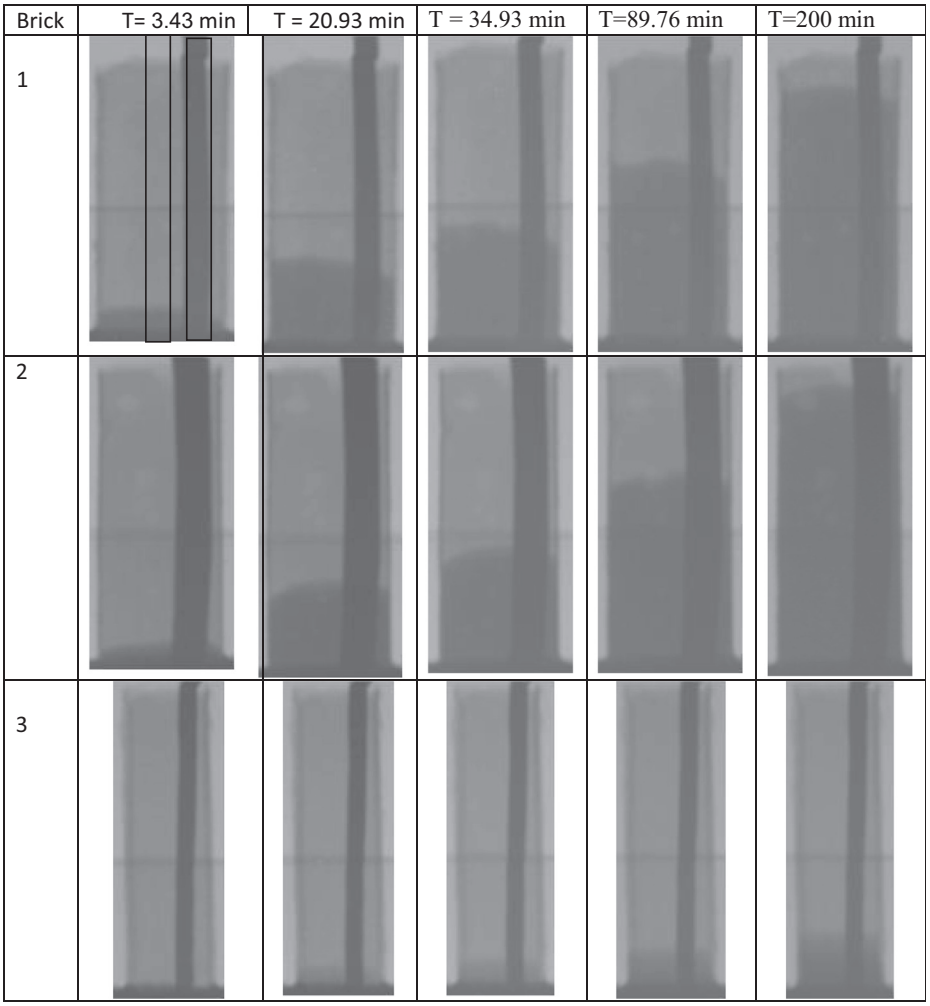

Fig. 1a. Neutron radiography images for brick samples 1, 2 and 3 at different absorption times (T).

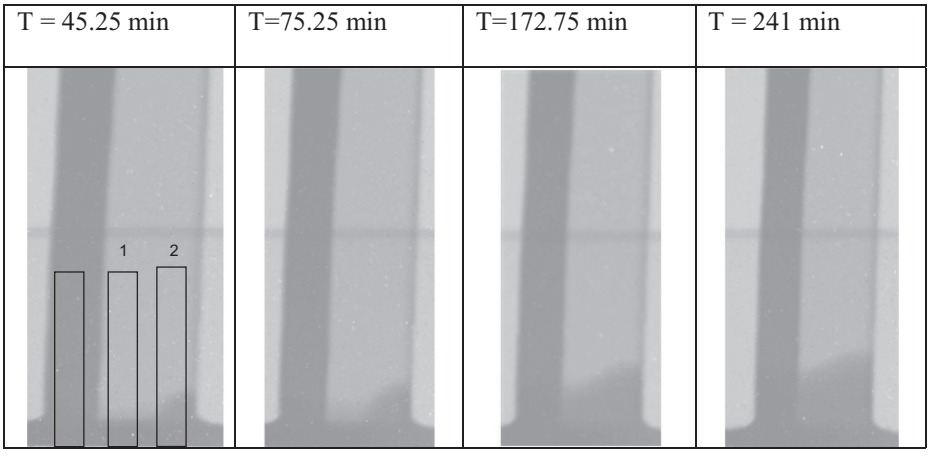

Fig. 1b. Neutron radiography images for brick 3 sample at different absorption times (T) in El Abd et al., 2020 [12]

mental ones (k) with maximum deviations less than ~ 15%. This means that the capillary coefficients for the investigated brick samples can be predicted from known values of sorptivity and capillary porosity. Sorpitivity can be determined from gravimetric measurements while capillary porosity can be determined by the water saturation method under atmospheric pressure.

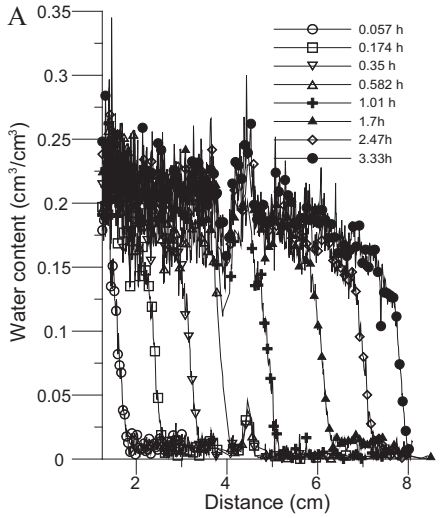

Fig. 2a. Water profiles for brick 1. The lines are guides for the eye.

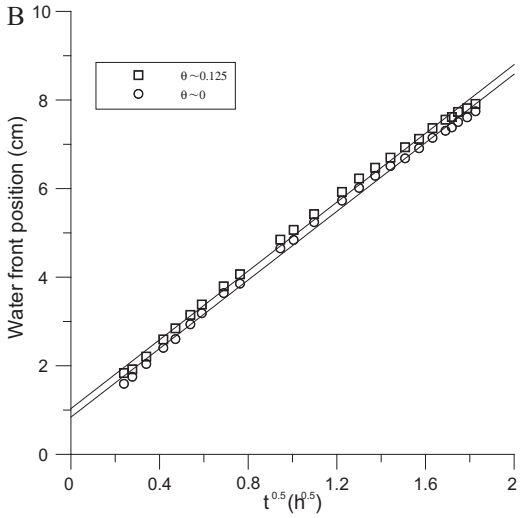

Fig. 2b. Water front position versus $\sqrt{t}$ for brick 1 along with straight equation fit lines.

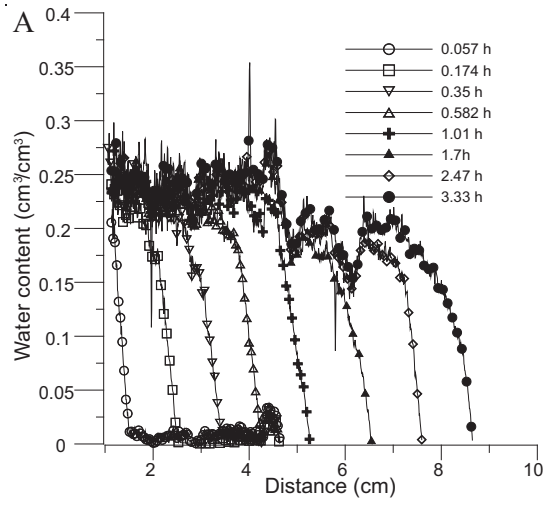

Fig. 3a. Water profiles for brick 2. The lines are guides for the eye.

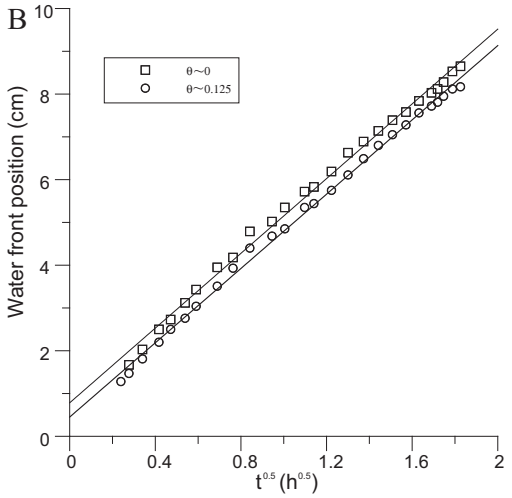

Fig. 3b. Water front position versus $\sqrt{t}$ for brick 2 along with straight equation fit lines.

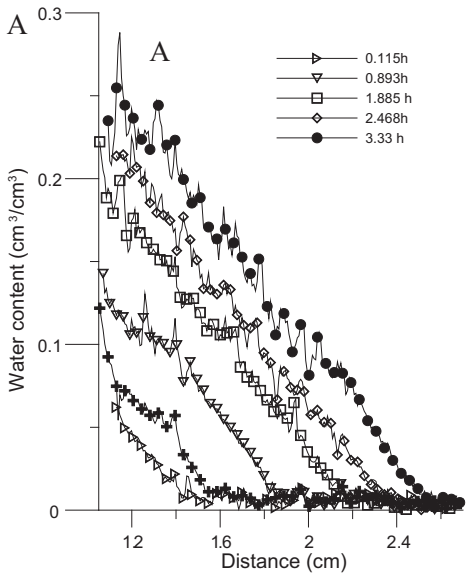

Fig. 4a. Water profiles for brick 3. The lines are guides for the eye.

3.3. Analysis of previous results

Experimental results from literature were collected for s, k and θ_c for cement-based materials, bricks and rocks. The values of k_c were calculated from reported values of s and θ_c ($k_c = s/\theta_c$) and compared with the measured ones, k. These results are listed in Table 2. Yang et al., 2019 [17] used X-ray CT to investigate the relationship between k and s of water for mortar and concrete samples. Values of k and s were determined by X-ray CT and the gravimetric method, respectively [17]. θ_c values were determined by the vacuum water-saturated method. Based on the result obtained and theoretical analysis, they have shown that the ratio of the ratio (s/k) equals the values of porosity [17]. Similarly, Zhang et al., 2011 [18] reported values of the same parameters using neutron radiography. There is correspondence between predicted and experimental values of k of the results reported by Yang et al., 2019 [17] and Zhang et al., 2011 [18] – Table 2. Pel et al., 1996 and references cited in [22] investigated moisture transport in brick and mortar samples using NMR. The values of k and θ_c were

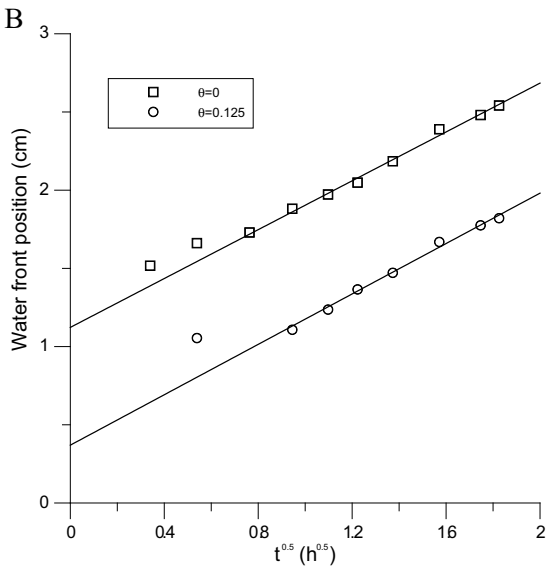

Fig. 4b. Water front position versus $\sqrt{t}$ for brick 3 along with straight equation fit lines.

reported for the investigated samples [22]. However, only some values for s determined by the gravimetric measurements were shown. Also, θ_c determined from vacuum saturation method were provided by the authors [22] - these values are not listed in Table 2. We have calculated the values of s from the (θ-ϕ) profiles and values of k (at half the value of θ_c). Values of k_c were calculated from both sorptivities determined using the (θ- ϕ) profiles and θ_c values reported. There is an agreement between predicted and experimental values of k. This means that the procedure used for determining sorptivities and using the values of θ_c , which are smaller than the corresponding ones determined by vacuum saturation method, are accurate and reliable from one hand and from the other hand such procedures credit results obtained in this work. Additionally, there is a deviation between calculated values of k (based on values of θ_c determined by vacuum saturation method) and the experimental values of k - these results are not shown. Similar calculations were carried out for the results reported for mortar samples [23,24]. These results were obtained by NMR and NR, respectively. θ_c, s and k (at half the value of θ_c) were determined from the (θ- ϕ) or θ-x profiles. Hall,1989 [25] reported (θ-ϕ) profiles of water absorption into a mortar bar (I: 3: 12 OPC/lime/sand by volume) obtained by NMR. From these results, we extracted the value of k. The values of s and θ_c measured by the gravimetric method were reported [25]. A gamma-ray attenuation was used to study water absorption into mortar at 20 °C, 35 °C, 45 ^{0}C and 55 ^{0}C [26]. Values of s, k and θ_c were determined from the θ-ϕ profiles provided by the authors. We did not determine the values of s, k and θ_c from the θ- ϕ profiles at the 55 ^{0}C since these profiles are not complete [26]. The determined value of θ_c = 0.145, corresponding to the highest values observed for the water content and less than the reported values (0.167), was considered equal to the value of θat ϕ = 0 [26] Leech et al., 2003 [27] showed that the values of θ_c determined by NMR for concrete samples were approximately equal to the value determined by vacuum saturation method. They reported the value of s (from the θ- ϕ profiles) and we determined the values of k (at half the value of θ_c) from the same profiles. Hazrati et al., 2002 [28] investigated water distribution in cement mortar mixtures using NMR under different drying conditions (oven and propan-2-ol drying). Results of θ_c and k were reported [28] and we determined the values of s and k (at half the value of θ_c) for only three oven dried samples from the reported θ-ϕ profiles. We could not deal with the other results since it was difficult to digitize them. Carmeliet et al., 2004 [29] investigated water absorption into calcium silicate plate and ceramic brick using x-ray radiography. We have determined values of s, k (at half the value of θ_c) from the θ- ϕ profiles reported and used θ_c provided by the authors [29]. Kang et al., 2013 [30] and Zhao et al., 2018 [31] investigated water absorption into Berea sandstone and tight samples by NR, respectively. They used the method of Meyer and Warrick, 1990 [32] to fit the θ- ϕ profiles. The fitting parameters including θ_c were used to determine the values of s and k. Generally, the predicted and experimental values for k for the reported results in references [23–31] are in good agreements. However, based on using reported values of θ_c = 0.167 [26] and reported value of k [27] deviations (less than 20%) can be noticed between predicted and reported experimental values of k. Carpenter et al., 1993 [33] used NMR to investigate water absorption in Lepine limestone (a typical constructional stone) and the value of k was reported. Values of s determined by both NMR and the gravimetric methods were found to be in agreement [33]. Also, it was noticed that the reported values of θ_c, determined by the vacuum saturation method, are in line with the estimated values determined from θ- ϕ profiles [33]. From these results [33], we have determined the values of k (at half the value of θ_c). Wang and Fang, 1988 [34] investigated moisture transport in sand column based on the traditional gravimetric method. The θ_c value was reported by authors [34] and we have calculated the values of s and k from the θ- ϕ profiles. It can be noticed that there is correspondence between the predicted and experimental values of k for the results reported in reference [34]. However, higher deviations can be noticed for the results reported in reference [33], especially when using reported k-value.

Table 1
Values of capillary penetration coefficients (k), sorptivities (s) and ratios (s/θ_c) in the present work and in El Abd et al., 2020 [12]

Brick	1	2	3	4[b]
k ($cm.h^{-0.5}$) [a]	3.88 ± 0.1 * 3.87 ± 0.1 **	4.36 ± 0.12* 4.34 ± 0.11**	0.781 ± 0.02* 0.806 ± 0.02**	–
k ($cm.h^{-0.5}$) [b]	2.64 ± 0.1	2.52 ± 0.07	Reg-1: 0.68 ± 0.017–0.700 ± 0.07 Reg-2: 0.500 ± 0.013	2.96 ± 0.1
Ratios of (k in this work/ k [12]	1.47	1.58	1.16 Reg-1 1.59 Reg-2	–
s ($cm.h^{-0.5}$)[a]	0.778 ± 0.08	0.964 ± 0.10	0.174 ± 0.017	
s ($cm.h^{-0.5}$) [b]	0.536 ± 0.06	0.491 ± 0.05	Reg-1: 0.155 ± 0.015 Reg-2: 0.114 ± 0.01	0.622 ± 0.07
θ_c^a	0.220 ± 0.02	0.25 ± 0.022	θ_c = 0.25 ± 0.027	
θ_c^b	0.220 ± 0.02	0.22 ± 0.020	θ_c = 0. 25 ± 0.027	0.220 ± 0.020
$(s/\theta_c)^a$	3.53 ± 0.33	3.86 ± 0.360	0.696 ± 0.08	–
$(s/\theta_c)^b$	2.44 ± 0.24	2.23 ± 0.210	Reg-1: 0.618 ± 0.07 Reg-2: 0.454 ± 0.050	2.83 ± 0.270

* at the θ = 0,** θ = 0.125 ,[a] this work, [b]El Abd et al., 2020 [12].

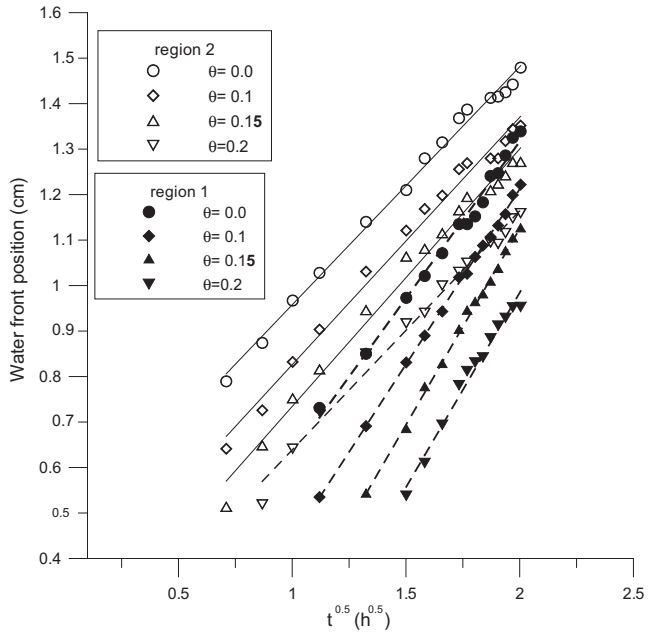

Fig. 5. Water front position versus $\sqrt{t}$ for brick 3 sample for regions 1 and 2 [12] along with straight equation fit lines.

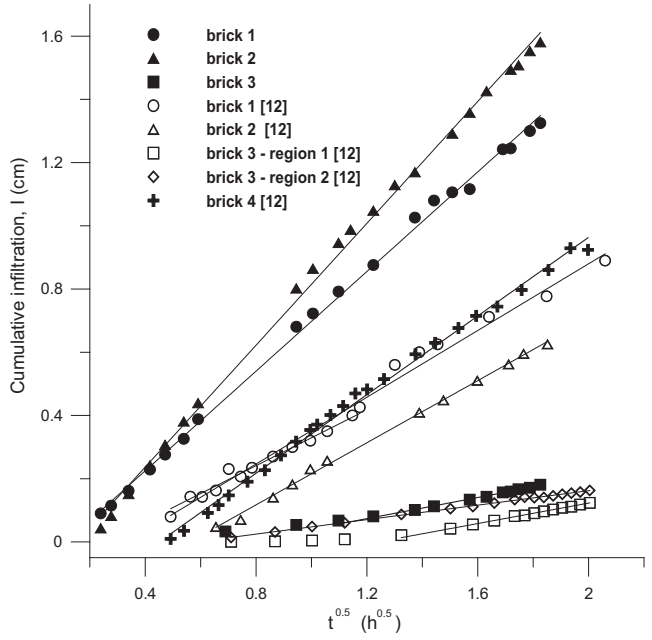

Fig. 6. Cumulative water infiltration (I) versus $\sqrt{t}$ for brick samples investigated in the present and previous work [12] along with straight equation fit lines.

Based on our results for brick samples and those shown in Table 2, it can be concluded that the value of k can be predicted from the measurements of capillary porosity and sorptivity determined by gravimetric measurements. Such approach can be applied as a satisfactory approximation, since it can be interpreted in terms of water flow in a single or a parallel bundle of capillary tubes [17–18]. It was reported that the capillary porosity is usually less than or equal to the vacuum saturated porosity in cement-based materials, however for bricks there is a significant difference between the two porosities [22,27].

To further check the procedures used in the present work for predicting the values of k, the values θ_c were determined by the gravimetric method for the brick samples investigated (samples were saturated by water under atmospheric pressure). The deviation between the determined θ_c values from the gravimetric measurement and NR method were found to be approximately 10% (values for θ_c determined by NR are smaller). To minimize such deviation and predict the values of k more precisely, capillary absorption tests were carried out for short brick samples for absorption times comparable to those of the NR experiments. Short samples were chosen to ensure that water fills the available pores for water flow such that the water content across the length of the samples is comparable. This was checked by weighting the samples after 3 h, 3.5 h and 4 h. It was found after an absorption time of 3 h that the weights of the samples are roughly constant. The deviation between the determined θ_c values from the gravimetric and NR measurements were found to be around 5%.

The approach used in this work, which is supported by experimental results, can be schematically represented by Figs. 7a, b and c. Fig. 7a shows the water profile characterized with sharp front. If the water front is very sharp, sorptivity (area under the curve) will be equal to the rectangle area ($k^* \theta_c$). However, sorptivity (s) is slightly less than that of the rectangle (area ~ $k^* \theta_c$) – Fig. 7a. More pronounced deviations can be noticed, as the sharpness of the water front decreases (Figs. 7b and c) and in such cases the values of sorptivities are lower than the areas of the rectangles ($k^* \theta_c$). Assuming water front position is at the mid value of θ_c, as shown by the dashed lines in Fig. 7a , b and c, deviations between s and $k^* \theta_c$ can be minimized. Such findings (s is lower than $k^* \theta_c$) explain the underestimated values of the predicted k values shown in Table 2.

The relationship between s and k [35–37] was investigated for cement-based materials considering the irregular shape of the pores (tortuosity and roundness). It was concluded that

$$s = \frac{\varphi}{c} k \qquad 11$$

where φ is porosity and c is a constant ($1 < c < 5$). The value of c depends on the porous matrix microstructure. In this work, the ratio $\frac{\varphi}{c}$ may interpreted as capillary porosity (θ_c) crediting results obtained in this work. Other fractal models describing water absorption in porous matrixes can be used and may lead to more reliable approaches explaining the relationship between s and k [35,38–40].

Neutron radiography was used to establish a relationship between capillary penetration coefficient and sorptivity for brick samples. Both parameters were determined from results extracted from acquired images. Moreover, the NR results showed that the capillary water absorption processes depend on the sealing material. The results obtained can be discussed in terms of the theory of unsaturated flow in porous media [12] where water diffusivities can be determined. In addition, it has been proved that artificial intelligence can be used as a potential substitution for typical traditional analytical methods for analyzing data of different neutron/photon radiation-based instruments [41–44]

4. Conclusion

Capillary water absorption into brick samples was measured using neutron radiography. The capillary penetration coefficient, sorptivity and capillary porosity were determined from the obtained results. It was proved that water sorptivity is directly proportional to capillary penetration coefficient for the brick samples

Table 2
Values of θ_c, s, and k collected from literature and calculated k_c for some porous materials.

Sample	s(cm.h$^{-1/2}$)	K(cm.h$^{-1/2}$)	θ_c	$k_c = s/\theta_c$	k_c/k	w/c	References
Mortar	0.194	0.990	0.200	0.97	0.98	0.45	Yang et al., 2019 [17]
Concrete	0.084	0.882	0.100	0.84	0.95	0.45	
Concrete	0.041	0.690	0.059	0.695	1.00	0.40	Zhang et al., 2011 [18]
Concrete	0.096	1.110	0.087	1.103	0.99	0.60	
RH	(1.621) 1.5	(8.88) 9.06	0.19	(8.53)[a] 7.89	(0.96)[a]0.87	–	Pel et al.,1996 and references cited in [22]
RZ	(2.362) 2.85	(9.42) 10.2	0.27	(8.747)[a] 10.75	(0.93)[a]1.05	–	
VE	(0.94) 3.3	(11.4) 12	0.28	(10.69)[a] 11.79	(0.94)[a] 0.9	–	
GH	(1.47) 1.56	(7.842) 8.52	0.20	(7.35)[a] 7.8	(0.94)[a]0.92	–	
Gz	(1.66) 2.22	(6.37) 8.22	0.27	(6.156)[a] 8.226	(0.97)[a] 1	–	
MM	0.728	4.902	0.16	4.552	0.93	–	
MZ	0.927	5.459	0.18	5.152	0.94	–	
sand-lime brick	0.466	1.848	0.27	1.725	0.93	–	
Gypsum(I)	0.906	3.360	0.29	3.124	0.93	–	
Mortar (oven dried)	0.267	1.788	0.155	1.665	0.93	0.40	Pel et al., 1998 [23]
Mortar	0.0234	0.187	0. 117	0.200	1.07	0.40	Zhang et al., 2017 [24]
Mortar	0.1120	0.770	0.160	0.700	0.91	0.60	
Mortar	1.99	8.78	0.27	7.37	0.84	0.50	Hall, 1989 [25]
Mortar (20 °C)	0.114	0.79	(0.167) 0.145	(0.680)[a] 0.78	(0.85)[a] 0.99	0.50	Daian,1988[26]
Mortar (35 °C)	0.096	0.685	(0.167) 0.145	(0.47)[a] 0.664	(0.84)[a] 0.97	0.50	
Mortar (35 °C)	0.116	0.864	(0.167) 0.145	(0.965)[a] 0.802	(0.8)[a] 0.93	0.50	
Mortar (45 °C)	0.100	0.747	(0.167) 0.145	(0.6)[a] 0.69	(0.8)[a] 0.92	0.50	
Concrete	0.15	1.308	0.126	1.19	0.91	0.40	Leech et al., 2003 [27]
Mortar (W60O)	0.424	(2.4) 2.10	0.210	2.019	(0.84)[a] 0.96	0.60	Hazrati et al., 2002 [28]
Mortar (W40O)	0.266	(1.98) 1.80	0.155	1.716	(0.87)[a] 0.95	0.40	
Mortar (W25O)	0.063	(0.77) 0.654	0.100	0.630	(0.82)[a] 0.96	0.25	
calcium silicate plate	7.61	10.00	0.81	9.4	0.92		Carmeliet et al., 2004 [29]
Ceramic brick	1.66	12.98	0.15	11.06	0.85		
A3	0.735	6.24	0.13	5.66	0.91		Kang et al., 2013 [30]
C3	0.537	4.92	0.11	4.88	1.00		
D2	0.613	5.7	0.12	5.11	0.90		
O3	0.930	7.878	0.13	7.16	0.91		
XT1	0.187	1.788	0.0906	2.062	1.15		Zhao et al., 2018 [31]
CT1	0.081	1.688	0.0540	1.494	0.88		
Lepine limestone	0.767	(4.52) 3.63	0.239	3.209	(0.71)[a] 0.88	–	Carpenter et al., 1993 [33]
Sand	8.22	43.00	0.200	41.12	0.96	–	Wang et al., 1988 [34]

Values of s, k and θ_c between brackets are calculated in this work from reported values in literature. [a] calculated based on the corresponding values of s, k and θ_c between brackets.

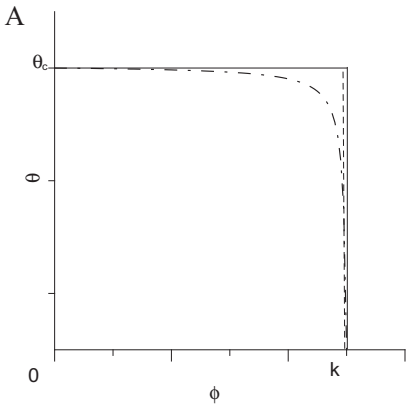

Fig.7a. sharp water front. The area under the curve (s) ~ $k^* \theta_c$.

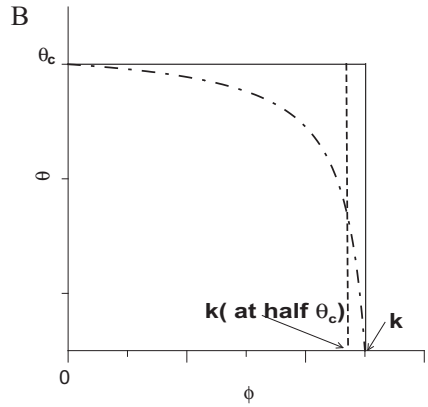

Fig.7b. The area under the curve (s) is lower than $k^* \theta_c$.

investigated and the proportionality constant is the capillary porosity. Such finding was confirmed by analyzing results in literature for many porous building materials. Capillary absorption coefficient (k) can be predicted with the knowledge of the capillary porosity and sorptivity which can be determined gravimetrically. The predicted values of k were found to agree with the experimental ones at half value of capillary porosity. Capillary absorption processes depend on the sealing materials used to cover the surface of the samples investigated. Acrylic paint as a sealing agent hampers the capillary absorption processes more effectively than the slurry adhesive coat.

CRediT authorship contribution statement

A. El Abd: Methodology, Formal analysis, Visualization, Investigation, Software, Data curation, Resources, Writing - original draft. **M. Taman:** Conceptualization, Methodology, Formal analysis, Visualization, Investigation, Software, Resources, Data curation, Writing - original draft, Writing - review & editing, Supervision. **S.E. Kichanov:** Methodology, Formal analysis, Visualization, Investigation, Software, Data curation, Resources, Writing - review & editing. **E. Hamad:** Formal analysis, Investigation, Software, Data

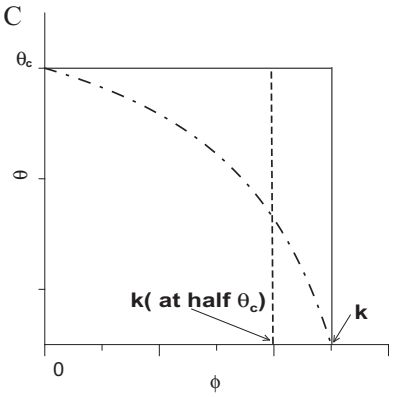

Fig. 7c. The area under the curve (s) is much lower than k* θ_c.

curation, Writing - original draft. K.**M. Nazarov:** Software, Visualization, Investigation, Data curation, Resources.

Declaration of Competing Interest

The authors declare that they have no known competing financial interests or personal relationships that could have appeared to influence the work reported in this paper.

Acknowledgments

The authors gratefully acknowledge the financial support from the Academy of Scientific Research and Technology (ASRT), Egypt. The results presented in this work is a part of the collaboration project between ASRT (Egypt) and National Natural Science Foundation of China (NSFC, Grant No. 51861145403). The Joint Institute for Nuclear Research (JINR), Dubna, Russia is gratefully acknowledged for performing neutron radiography experiments. Prof. Yixin Zhao (China University of Mining and Technology) is highly acknowledged for his useful comments and discussions during the preparation of this work.

References

[1] H. Pleinert, H. Sadouki, F.H. Wittmann, Determination of moisture distributions in porous building materials by neutron transmission analysis, Mater. Struct. 31 (4) (1998) 218–224, https://doi.org/10.1007/bf02480418.
[2] T. Nemec, J. Rant, V. Apih, B. Glumac, Study of building materials impregnation processes by quasi-real-time neutron radiography, Nucl. Instrum. Methods Phys. Res., Sect. A 424 (1) (1999) 242–247, https://doi.org/10.1016/s0168-9002(98)01301-1.
[3] M. Janz, Moisture diffusivities evaluated at high moisture levels from a series of water absorption tests, Mater. Struct. 35 (3) (2002) 141–148, https://doi.org/10.1007/bf02533582.
[4] J. Schoelkopf, P.A. Gane, C.J. Ridgway, G.P. Matthews, Practical observation of deviation from Lucas-Washburn scaling in porous media, Colloids Surf., A 206 (1–3) (2002) 445–454, https://doi.org/10.1016/s0927-7757(02)00066-3.
[5] C. Feng, H. Janssen, Hygric properties of porous building materials (III): Impact factors and data processing methods of the capillary absorption test, Build. Environ. 134 (2018) 21–34, https://doi.org/10.1016/j.buildenv.2018.02.038.
[6] C. David, D. Bertauld, J. Dautriat, J. Sarout, B. Menéndez, B. Nabawy, Detection of moving capillary front in porous rocks using X-ray and ultrasonic methods, Front. Phys. 3 (2015) 53, https://doi.org/10.3389/fphy.2015.00053.
[7] B.S. Nabawy, C. David, X-Ray CT scanning imaging for the Nubia sandstones: A macro scale tool for characterizing fluid transport, Geosci. J. 20 (5) (2016) 691–704, https://doi.org/10.1007/s12303-015-0073-7.
[8] A.A. Harms, D.R. Wyman, Mathematics and Physics of Neutron, Radiography. (1986), https://doi.org/10.1007/978-94-015-6937-8.
[9] P. Zhang, F.H. Wittmann, P. Lura, H.S. Müller, S. Han, T. Zhao, Application of neutron imaging to investigate fundamental aspects of durability of cement-based materials: a review, Cem. Concr. Res. 108 (2018) 152–166, https://doi.org/10.1016/j.cemconres.2018.03.003.
[10] E. Perfect, C.L. Cheng, M. Kang, H.Z. Bilheux, J.M. Lamanna, M.J. Gragg, D.M. Wright, Neutron imaging of hydrogen-rich fluids in geomaterials and engineered porous media: A review, Earth Sci. Rev. 129 (2014) 120–135, https://doi.org/10.1016/j.earscirev.2013.11.012.
[11] Y. Zhao, Y. Wu, S. Han, S. Xue, G. Fan, Z. Chen, A. El Abd, Water sorptivity of unsaturated fractured sandstone: Fractal modeling and neutron radiography experiment, Adv. Water Resour. 130 (2019) 172–183, https://doi.org/10.1016/j.advwatres.2019.06.006.
[12] A. El Abd, S.E. Kichanov, M. Taman, K.M. Nazarov, D.P. Kozlenko, Wael M. Badawy, Determination of moisture distributions in porous building bricks by neutron radiography, Appl. Radiat. Isot. 156 (2020) 108970, https://doi.org/10.1016/j.apradiso.2019.108970.
[13] A. El Abd, A. Czachor, J. Milczarek, Neutron radiography determination of water diffusivity in fired clay brick, Appl. Radiat. Isot. 67 (4) (2009) 556–559, https://doi.org/10.1016/j.apradiso.2008.11.014.
[14] A.G. Abd, A. Czachor, J.J. Milczarek, J. Pogorzelski, Neutron radiography studies of water migration in construction porous materials, IEEE Trans. Nucl. Sci. 52 (1) (2005) 299–304, https://doi.org/10.1109/tns.2005.843642.
[15] A. Elabd, J.J. Milczarek, Neutron radiography study of water absorption in porous building materials: anomalous diffusion analysis, J. Phys. D Appl. Phys. 37 (16) (2004) 2305–2313, https://doi.org/10.1088/0022-3727/37/16/013.
[16] L. Hanžič, R. Ilić, Relationship between liquid sorptivity and capillarity in concrete, Cem. Concr. Res. 33 (9) (2003) 1385–1388, https://doi.org/10.1016/s0008-8846(03)00070-x.
[17] Lin Yang, Danying Gao, Yunsheng Zhang, Jiyu Tang, Ying Li, Relationship between sorptivity and capillary coefficient for water absorption of cement-based materials: theory analysis and experiment, R. Soc. Open Sci. 6 (6) (2019) 190112, https://doi.org/10.1098/rsos.190112.
[18] P. Zhang, F.H. Wittmann, T.J. Zhao, E.H. Lehmann, P. Vontobel, Neutron radiography, a powerful method to determine time-dependent moisture distributions in concrete, Nucl. Eng. Des. 241 (12) (2011) 4758–4766, https://doi.org/10.1016/j.nucengdes.2011.02.031.
[19] D. Kozlenko, Neutron imaging facility at IBR-2 high flux pulsed reactor: first results, in: 10th World Conference on Neutron Radiography. Grindelwald, 2014, p. 27.
[20] D.P. Kozlenko, S.E. Kichanov, E.V. Lukin, A.V. Rutkauskas, A.V. Belushkin, G.D. Bokuchava, B.N. Savenko, Neutron radiography and tomography facility at IBR-2 reactor, Phys. Part. Nucl. Lett. 13 (3) (2016) 346–351, https://doi.org/10.1134/s1547477116030146.
[21] C.A. Schneider, W.S. Rasband, K.W. Eliceiri, NIH Image to ImageJ: 25 years of image analysis, Nat. Methods 9 (7) (2012) 671–675, https://doi.org/10.1038/nmeth.2089.
[22] L. Pel, K. Kopinga, H.J.P. Brocken, Moisture transport in porous building materials, Heron 41 (2) (1996) 95–105.
[23] L. Pel, K. Hazrati, K. Kopinga, J. Marchand, Water absorption in mortar determined by NMR, Magn. Reson. Imaging 16 (5–6) (1998) 525–528, https://doi.org/10.1016/s0730-725x(98)00061-7.
[24] P. Zhang, D. Hou, Q. Liu, Z. Liu, J. Yu, Water and chloride ions migration in porous cementitious materials: An experimental and molecular dynamics investigation, Cem. Concr. Res. 102 (2017) 161–174, https://doi.org/10.1016/j.cemconres.2017.09.010.
[25] C. Hall, Water sorptivity of mortars and concretes: a review, Mag. Concr. Res. 41 (147) (1989) 51–61, https://doi.org/10.1680/macr.1989.41.147.51.
[26] J.-F. Daian, Condensation and isothermal water transfer in cement mortar Part I ? Pore size distribution, equilibrium water condensation and imbibition, Transp. Porous Media 3 (6) (1988) 563–589, https://doi.org/10.1007/bf00959103.
[27] C. Leech, Unsaturated diffusivity functions for concrete derived from NMR images, Mater. Struct. 36 (260) (2003) 413–418, https://doi.org/10.1617/13760.
[28] K. Hazrati, L. Pel, J. Marchand, K. Kopinga, M. Pigeon, Determination of isothermal unsaturated capillary flow in high performance cement mortars by NMR imaging, Mater. Struct. 35 (10) (2002) 614–622, https://doi.org/10.1007/bf02480354.
[29] J. Carmeliet, H. Hens, S. Roels, O. Adan, H. Brocken, R. Cerny, Z. Pavlik, C. Hall, K. Kumaran, L. Pel, Determination of the liquid water diffusivity from transient moisture transfer experiments, J. Therm Envelope Build Sci. 27 (4) (2004) 277–305, https://doi.org/10.1177/1097196304042324.
[30] Kang, M., Perfect, E., Cheng, C.L., Bilheux, H.Z., Gragg, M., Wright, D.M., Lamanna, J.M., Horita, J. and Warren, J.M., 2013. Diffusivity and sorptivity of Berea sandstone determined using neutron radiography. Vadose Zone J., 12(3). http://dx.doi.org/10.2136/vzj2012.0135.
[31] Y. Zhao, S. Xue, S. Han, L. He, Z. Chen, Characterization of unsaturated diffusivity of tight sandstones using neutron radiography, Int. J. Heat Mass Transf. 124 (2018) 693–705, https://doi.org/10.1016/j.ijheatmasstransfer.2018.03.090.
[32] J.J. Meyer, A.W. Warrick, Analytical Expression for Soil Water Diffusivity Derived from Horizontal Infiltration Experiments, Soil Sci. Soc. Am. J. 54 (6) (1990) 1547–1552, https://doi.org/10.2136/sssaj1990.03615995005400060006x.
[33] T.A. Carpenter, E.S. Davies, C. Hall, L.D. Hall, W.D. Hoff, M.A. Wilson, Capillary water migration in rock: process and material properties examined by NMR imaging, Mater. Struct. 26 (5) (1993) 286–292, https://doi.org/10.1007/BF02472950.
[34] Wang, B., Zhao-Hong, F., 1988. Water absorption and measurement of the mass diffusivity in porous media. International Journal of Heat and Mass Transfer, 31(2), pp.251–257. Available at: http://dx.doi.org/10.1016/0017-9310(88)90007-5.

[35] Haitao Zhao, Jian Ding, Yuyu Huang, Yimin Tang, Wen Xu, Donghui Huang, Experimental analysis on the relationship between pore structure and capillary water absorption characteristics of cement-based materials, Structural Concrete 20 (5) (2019) 1750–1762, https://doi.org/10.1002/suco.v20.510.1002/suco.201900184.
[36] Haitao Zhao, Jian Ding, Yuyu Huang, Guodong Xu, Wei Li, Shiping Zhang, Penggang Wang, Investigation on sorptivity and capillarity coefficient of mortar and their relationship based on microstructure, Constr. Build. Mater. 265 (2020) 120332, https://doi.org/10.1016/j.conbuildmat.2020.120332.
[37] D. Benavente, P. Lock, M.Á.G. Del Cura, S. Ordóñez, Predicting the capillary imbibition of porous rocks from microstructure, Transp. Porous Media 49 (1) (2002) 59–76, https://doi.org/10.1016/j.enggeo.2015.06.003.
[38] G. Pia, C. Siligardi, L. Casnedi, U. Sanna, Pore size distribution and porosity influence on Sorptivity of ceramic tiles: From experimental data to fractal modelling, Ceram. Int. 42 (8) (2016) 9583–9590, https://doi.org/10.1016/j.ceramint.2016.03.041.
[39] G. Pia, U. Sanna, An intermingled fractal units model to evaluate pore size distribution influence on thermal conductivity values in porous materials, Appl. Therm. Eng. 65 (1–2) (2014) 330–336, https://doi.org/10.1016/j.applthermaleng.2014.01.037.
[40] Xiaohui Zeng, Lou Chen, Keren Zheng, Chenbo Ling, Huasheng Zhu, Haichuan Liu, Ping Wang, Kunpeng Li, Zhicheng Liu, Ming Wang, Electrical resistivity and capillary absorption in mortar with styrene-acrylic emulsion and air-entrained agent: improvement and correlation with pore structure, Constr. Build. Mater. 255 (2020) 119287, https://doi.org/10.1016/j.conbuildmat.2020.119287.
[41] S. Arezki, Implementation of a Neutron Imaging Decision Support System (NDSS), Electrotehnica, Electronica, Automatica 65 (3) (2017) 183–190.
[42] Mohammadmehdi Roshani, Giang T.T. Phan, Peshawa Jammal Muhammad Ali, Gholam Hossein Roshani, Robert Hanus, Trung Duong, Enrico Corniani, Ehsan Nazemi, El Mostafa Kalmoun, Evaluation of flow pattern recognition and void fraction measurement in two phase flow independent of oil pipeline's scale layer thickness, Alexan. Eng. J. 60 (1) (2021) 1955–1966, https://doi.org/10.1016/j.aej.2020.11.043.
[43] Hossein Mehnatkesh, Aria Alasty, Mehrdad Boroushaki, Mohammad Hassan Khodsiani, Mohammad Reza Hasheminasab, Mohammad Jafar Kermani, Estimation of Water Coverage Ratio in Low Temperature PEM-Fuel Cell Using Deep Neural Network, IEEE Sens. J. 20 (18) (2020) 10679–10686, https://doi.org/10.1109/JSEN.736110.1109/JSEN.2020.2993181.
[44] M. Roshani, G. Phan, G.H. Roshani, G. Hossein, R. Hanus, B. Bazemi, E. Corniani, E. Nazemi, Combination of X-ray tube and GMDH neural network as a nondestructive and potential technique for measuring characteristics of gas-oil-water three phase flows, Measurement 168 (2021), https://doi.org/10.1016/j.measurement.2020.108427 108427.